*Int. J. Heat Mass Transfer.* Vol. 27, No. 11, pp. 2057–2066, 1984
Printed in Great Britain

0017 9310/84 $3.00 + 0.00
Pergamon Press Ltd.

# Analysis of heat transfer during melting from a vertical wall

M. OKADA

Department of Mechanical Engineering, Aoyamagakuin University, Setagaya-ku, Tokyo 157, Japan

(*Received* 25 *January* 1984)

**Abstract**—A vertical boundary of a horizontal plate-like solid initially at the fusion temperature with adiabatic upper and lower surfaces was subjected to a step-wise temperature increase. The resulting melting process with natural convection in the time-dependent melt region was analyzed by means of a finite-difference method. Analytical results of the shape of the melting front and the temperature distribution in the melt region agreed well with the experimental results by using n-octadecane as a phase change material, which had been presented by the author. A simple relationship between the average Nusselt number along the vertical wall and dimensionless time was obtained.

## 1. INTRODUCTION

A FUNDAMENTAL understanding of heat transfer during melting and solidification is required for efficient design of latent heat-of-fusion energy storage systems. The effect of natural convection in the melt region is of particular importance in such phase change problems, especially in the melting process. The heat transfer along the solid–liquid interface by natural convection changes the position and shape of the solid–liquid interface. Such a problem has recently been actively studied. Basic studies have been concerned with melting processes from heat input along various surfaces of a phase change material (PCM). The majority of these studies were based on experiments [1–7]. Analytical results have not been reported except for limited problems because the moving boundary makes the problems complex and it is difficult to converge the solution of the natural convection with high Rayleigh number. Melting around a vertical circular cylinder [8], melting around a horizontal circular cylinder [9], and melting in a horizontal circular cylinder [10, 11] have been analyzed numerically. A perturbation solution on the melting around a horizontal cylinder, which was available in a very short period of melting, has been obtained [12]. As ref. [8] was the first analysis of multidimensional unsteady natural convection phase change, the governing equations had some approximations. Therefore, their analysis was available when the solid–liquid interface had a small gradient to the vertical direction. Melting from a vertical wall has been studied by means of experiments only [5–7]. In a previous paper experiments were carried out on such a melting process over a large range of width to height ratios of PCM geometries and a dimensionless correlation between thermal energy storage and some parameters of melting was obtained [7].

The objectives of the present study were to establish an analysis of the melting from a vertical wall and to get a clear understanding of the roles of natural convection in the melt region. In the present study, as shown schematically in Fig. 1, two-dimensional melting in a rectangular enclosure was analyzed by means of a finite-difference method. A vertical wall between insulated top and bottom surfaces is heated so as to produce a step-wise temperature change; the other vertical wall is located far enough away from the heated wall so as not to influence the melting process. A PCM is initially solid at the fusion temperature. Such a problem was solved by a finite-difference method under the quasi-steady state assumption. Solutions were obtained for Rayleigh numbers up to $5 \times 10^6$ and the width to height ratio of PCM up to 1 or 3. Before formulating the finite-difference equations, the variables in the governing equations were transformed twice in order to fix the moving boundary and divide the real space near the boundaries into a grid of sufficient small sizes. The analytical results of the melting front and the temperature distribution along the centerline of the enclosure were compared with the experimental results presented before [7]. Both the variations of the dimensionless thermal energy stored as latent heat and the average Nussselt number on the vertical wall with the dimensionless time were obtained by analysis and expressed by simple equations.

## 2. ANALYSIS

### 2.1. *Governing equations*

Natural convection in the melt region is considered to be laminar and two-dimensional. The Boussinesq approximation is assumed to be valid and the viscous

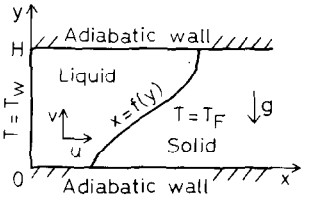


FIG. 1. Schematic of two-dimensional melting process.

## NOMENCLATURE

$a_1, a_2, \ldots, a_5, A_1, A_2, \ldots, A_6$ coefficients in the transformed equations, equations (10)–(12)
A, B, C, D, E, F, G differential operators in equations (16)–(20)
$B_k(\tau)$ coefficient of the polynomial function defined by equation (21)
$c$ specific heat of liquid phase
$C$ coefficient of $\overline{Nu}_W$ represented by equation (26)
$f, f(y, t)$ location of the melting front
$F, F(Y, \tau), F(Y, Fo)$ dimensionless location of the melting front, $f/H$
$Fo$ Fourier number, $\alpha t/H^2$
$\Delta Fo$ interval of Fourier number to solve the vorticity equation, equation (17)
$\Delta Fo^*$ critical interval of Fourier number which converges the explicit finite-difference equation for equation (16)
$g$ gravitational acceleration
$h$ heat transfer coefficient
$\Delta h$ latent heat of fusion
$H$ height of the vertical wall
$k$ thermal conductivity of liquid phase
$K$ degree number of the polynomial function, equation (21)
$M, N$ division numbers of the melt region in $\zeta$, $Y$ direction
$Nu$ Nusselt number, $hH/k$
$Pr$ Prandtl number, $\nu/\alpha$
$Q_l$ thermal energy storage as latent heat per unit depth of enclosure
$Q_l^*$ dimensionless thermal energy storage as latent heat, $Q_l/(\Delta h \rho H^2) = \bar{F}$
$Ra$ Rayleigh number, $g\beta(T_W - T_F)H^3\ Pr/\nu^2$
$Ste$ Stefan number, $c(T_W - T_F)/\Delta h$
$t$ time
$T$ temperature
$u, v$ velocities in $x$, $y$ direction
$U, V$ dimensionless velocities in $X$, $Y$ direction, respectively, $Hu/\nu$, $Hv/\nu$
$(x, y)$ Cartesian coordinates
$(X, Y)$ dimensionless Cartesian coordinates, respectively, $x/H$, $y/H$
$\Delta Y$ increment of $Y$ coordinate.

Greek symbols
$\alpha$ thermal diffusivity of liquid phase
$\beta$ thermal expansion coefficient
$\gamma$ rate of deviation from steady-state solution
$\varepsilon_\theta, \varepsilon_\Psi, \varepsilon_\Omega$ criterions of convergence by the Gauss–Seidel iteration method
$\zeta$ transformed variable defined by equations (7)–(9)
$\Delta\zeta$ increment of $\zeta$ coordinate
$\theta$ dimensionless temperature, $(T - T_F)/(T_W - T_F)$
$\lambda$ ratio of time interval, $\Delta Fo/\Delta Fo^*$
$\nu$ kinematic viscosity
$\xi$ transformed variable, $X/F(Y)$
$\rho$ density
$\sigma$ root of equation (23)
$\tau$ dimensionless time, $Fo\ Ste$
$\Delta\tau$ dimensionless time interval to get a new location of the melting front
$\psi$ stream function
$\Psi$ dimensionless stream function, $\psi/\nu$
$\omega$ vorticity
$\Omega$ dimensionless vorticity, $H^2\omega/\nu$
$\Omega^s$ solution of steady-state vorticity equation.

Subscripts
F solid–liquid interface or fusion
$j$ time step determining the melting front location
L average at left and central nodal points
$(m, n)$ position of nodal points, $\zeta = (m-1)\Delta\zeta$, $Y = (n-1)\Delta Y$
R average at right and central nodal points
t transition time from conduction domain to natural convection domain
W vertical wall.

Superscripts
$i$ time step to get a steady-state natural convection
$\bar{}$ mean value
$'$ value at the next step by the Gauss–Seidel iteration method.

heat dissipation is neglected. The temperature of the vertical wall is maintained at $T_W$. The location of melting front at time $t$ is represented by $x = f(y, t)$. The non-steady governing equations in the melt region; i.e. the vorticity transport equation, the energy conservation equation, the relationship between the vorticity and the stream function, and the definitions of the stream function are respectively given in dimensionless form as

$$\frac{\partial\Omega}{\partial Fo} + Pr\left(U\frac{\partial\Omega}{\partial X} + V\frac{\partial\Omega}{\partial Y}\right) = Pr\ \nabla^2\Omega + Ra\frac{\partial\theta}{\partial X} \quad (1)$$

$$\frac{\partial\theta}{\partial Fo} + Pr\left(U\frac{\partial\theta}{\partial X} + V\frac{\partial\theta}{\partial Y}\right) = \nabla^2\theta \quad (2)$$

$$\nabla^2\Psi = -\Omega \quad (3)$$

$$U = \frac{\partial \Psi}{\partial Y}, \quad V = -\frac{\partial \Psi}{\partial X} \tag{4}$$

where $\nabla^2$ is a two-dimensional Laplacian operator defined as

$$\nabla^2 = \frac{\partial^2}{\partial X^2} + \frac{\partial^2}{\partial Y^2}.$$

Boundary conditions are

$$U = V = 0, \quad \Psi = 0 \quad \text{at} \quad X = 0,$$

$$X = F(Y, Fo), \quad Y = 0, \quad Y = 1;$$

$$\theta = 1 \quad \text{at} \quad X = 0 \quad \theta = 0 \quad \text{at} \quad X = F(Y, Fo),$$

$$\frac{\partial \theta}{\partial Y} = 0 \quad \text{at} \quad Y = 0, \quad Y = 1;$$

$$\Omega = -\frac{\partial^2 \Psi}{\partial X^2} \quad \text{at} \quad X = 0,$$

$$\Omega = -\left\{1 + \left(\frac{\partial F}{\partial Y}\right)^2\right\} \frac{\partial^2 \Psi}{\partial X^2} \quad \text{at} \quad X = F(Y, Fo),$$

$$\Omega = -\frac{\partial^2 \Psi}{\partial Y^2} \quad \text{at} \quad Y = 0, \quad Y = 1.$$

The dimensionless variables and parameters are defined as

$$\Omega = \frac{H^2 \omega}{\nu}, \quad \theta = \frac{T - T_F}{T_W - T_F}, \quad \Psi = \frac{\psi}{\nu},$$

$$U = \frac{Hu}{\nu}, \quad V = \frac{Hv}{\nu}, \quad X = \frac{x}{H},$$

$$Y = \frac{y}{H}, \quad Fo = \frac{\alpha t}{H^2}, \quad F(Y, Fo) = \frac{f(y,t)}{H},$$

$$Ra = \frac{g\beta(T_W - T_F)H^3}{\nu^2} Pr, \quad Pr = \frac{\nu}{\alpha}.$$

The time-wise evolution of the melting front is determined by the energy balance at the solid–liquid interface. By neglecting the density change between solid and liquid phases

$$\frac{\partial F}{\partial Fo} = -Ste\left(\frac{\partial \theta}{\partial X} - \frac{\partial F}{\partial Y}\frac{\partial \theta}{\partial Y}\right) \tag{5}$$

where $Ste = c(T_W - T_F)/\Delta h$ is the Stefan number. In the case of small Stefan number, the melting front moves relatively slowly. Then the natural convection in the melt region can be treated as quasi-steady during the melting process. Therefore, the derivatives of vorticity and temperature with respect to time in equations (1) and (2) drop out and only one parameter involving time is found, i.e. $Fo\ Ste$ in equation (5).

Equations (1)–(4) were solved for steady-state solutions at every time step by means of the variable transformation technique. First the melt region was changed into a simple rectangular region by transforming the independent variable $X$ to $\xi$

$$\xi = X/F(Y) \tag{6}$$

where the location of the melting front $F$ was treated as a function of $Y$ only, due to the quasi-steady state assumption. Furthermore, in order to divide the real space near the boundaries of $X = 0$ and $F(Y)$ into a grid of sufficient small sizes, the second variable transformation $\zeta = \zeta(\xi)$ was carried out. The following three expressions were used for $\zeta$

$$\zeta = \xi \tag{7}$$

$$\zeta = 12(\xi - \tfrac{1}{2})^5 + \tfrac{1}{4}(\xi - \tfrac{1}{2}) + \tfrac{1}{2} \tag{8}$$

$$\zeta = 56(\xi - \tfrac{1}{2})^7 + \tfrac{1}{8}(\xi - \tfrac{1}{2}) + \tfrac{1}{2}. \tag{9}$$

When the width of the melt region is very thin, equation (7) was used and according to the thickness of the boundary layer by natural convection equation (8) or equation (9) was used. Consequently equations (1)–(4) are transformed as follows

$$Pr\left(A_1 \frac{\partial^2 \Omega}{\partial \zeta^2} + A_2 \frac{\partial \Omega}{\partial \zeta} + A_4 \frac{\partial \Omega}{\partial Y} + \frac{\partial^2 \Omega}{\partial Y^2}\right) = \frac{\partial \Omega}{\partial Fo} - \frac{Ra}{F}\frac{d\zeta}{d\xi}\frac{\partial \theta}{\partial \zeta} + Pr\, A_3 \frac{\partial^2 \Omega}{\partial \zeta \partial Y} \tag{10}$$

$$A_1 \frac{\partial^2 \theta}{\partial \zeta^2} + A_5 \frac{\partial \theta}{\partial \zeta} + Pr\, A_4 \frac{\partial \theta}{\partial Y} + \frac{\partial^2 \theta}{\partial Y^2} = A_3 \frac{\partial^2 \theta}{\partial \zeta \partial Y} \tag{11}$$

$$A_1 \frac{\partial^2 \Psi}{\partial \zeta^2} + A_6 \frac{\partial \Psi}{\partial \zeta} + \frac{\partial^2 \Psi}{\partial Y^2} = A_3 \frac{\partial^2 \Psi}{\partial \zeta \partial Y} - \Omega \tag{12}$$

$$U = V\xi \frac{dF}{dY} + \frac{\partial \Psi}{\partial Y}, \quad V = -\frac{1}{F}\frac{d\zeta}{d\xi}\frac{\partial \Psi}{\partial \zeta} \tag{13}$$

where

$$A_1 = a_1\left(\frac{d\zeta}{d\xi}\right)^2, \quad A_2 = a_1\frac{d^2\zeta}{d\xi^2} + a_5\frac{d\zeta}{d\xi},$$

$$A_3 = 2a_3\frac{d\zeta}{d\xi}, \quad A_4 = -V,$$

$$A_5 = a_1\frac{d^2\zeta}{d\xi^2} + a_4\frac{d\zeta}{d\xi}, \quad A_6 = a_1\frac{d^2\zeta}{d\xi^2} + a_2\frac{d\zeta}{d\xi};$$

$$a_1 = \frac{1}{F^2}\left\{1 + \left(\xi\frac{dF}{dY}\right)^2\right\}, \quad a_2 = \frac{\xi}{F}\left\{\frac{2}{F}\left(\frac{dF}{dY}\right)^2 - \frac{d^2F}{dY^2}\right\},$$

$$a_3 = \frac{\xi}{F}\frac{dF}{dY}, \quad a_4 = a_2 - \frac{Pr}{F}\frac{\partial \Psi}{\partial Y}, \quad a_5 = a_2 - \frac{1}{F}\frac{\partial \Psi}{\partial Y}.$$

The boundary conditions are

$$\Psi = 0, \quad U = V = 0 \quad \text{at} \quad \zeta = 0,$$

$$\zeta = 1, \quad Y = 0, \quad Y = 1;$$

$$\theta = 1 \quad \text{at} \quad \zeta = 0, \quad \theta = 0 \quad \text{at} \quad \zeta = 1,$$

$$\partial\theta/\partial Y = 0 \quad \text{at} \quad Y = 0, \quad Y = 1;$$

$$\Omega = -\frac{1}{F^2}\left(\frac{d\zeta}{d\xi}\right)^2 \frac{\partial^2 \Psi}{\partial \zeta^2} \quad \text{at} \quad \zeta = 0,$$

$$\Omega = -\frac{1}{F^2}\left\{1 + \left(\frac{dF}{dY}\right)^2\right\}\left(\frac{d\zeta}{d\xi}\right)^2 \frac{\partial^2 \Psi}{\partial \zeta^2} \quad \text{at} \quad \zeta = 1;$$

$$\Omega = -\frac{\partial^2 \Psi}{\partial Y^2} \quad \text{at} \quad Y = 0, \quad Y = 1.$$

The derivative of vorticity with respect to time in equation (10) is left because of the necessity for converging the solution. The coefficients $A_1$ and $A_3$ are known but the $A_2$, $A_4$, $A_5$, and $A_6$ coefficients contain unknown variables $U$ and/or $V$.

The energy balance equation (5) at the solid–liquid interface is transformed as

$$\frac{\partial F}{\partial \tau} = -\frac{1}{F}\left\{1+\left(\frac{\partial F}{\partial Y}\right)^2\right\}\left[\frac{\mathrm{d}\zeta}{\mathrm{d}\xi}\right]_{\xi=1}\left[\frac{\partial \theta}{\partial \zeta}\right]_{\zeta=1} \tag{14}$$

where the dimensionless time $\tau$ is

$$\tau = Fo\ Ste. \tag{15}$$

2.2. *Finite difference formulation and procedure of solution for natural convection*

The transformed coordinate $\zeta$ was divided into $M$ equal segments and $Y$ divided into $N$. Then $\Delta\zeta = 1/M$ and $\Delta Y = 1/N$. Subscripts $(m, n)$ refer to the location of nodal point: $\zeta = (m-1)\Delta\zeta$ $(m = 1, 2, \ldots, M+1)$ and $Y = (n-1)\Delta Y (n = 1, 2, \ldots, N+1)$. The finite-difference equations for equations (10)–(13) were formulated as the following examples. For the second derivatives

$$\frac{\partial^2 \Omega}{\partial \zeta^2} = \frac{\Omega_{m+1,n} - 2\Omega_{m,n} + \Omega_{m-1,n}}{(\Delta\zeta)^2}$$

$$\frac{\partial^2 \Omega}{\partial \zeta \partial Y} = \frac{\Omega_{m+1,n+1} - \Omega_{m+1,n-1} - \Omega_{m-1,n+1} + \Omega_{m-1,n-1}}{4\Delta\zeta\Delta Y}.$$

The second up-wind differencing method [13] was adopted for the first derivatives coupling with coefficients $A_2$, $A_4$, $A_5$, and $A_6$

$$A_2\frac{\partial \Omega}{\partial \zeta} = \frac{|A_{2R}| + A_{2R}}{2}\frac{\Omega_{m+1,n} - \Omega_{m,n}}{\Delta\zeta} + \frac{|A_{2L}| - A_{2L}}{2}\frac{\Omega_{m-1,n} - \Omega_{m,n}}{\Delta\zeta}$$

where

$$A_{2R} = (A_{2,m+1,n} + A_{2,m,n})/2,$$

$$A_{2L} = (A_{2,m-1,n} + A_{2,m,n})/2.$$

For the other first derivatives

$$\frac{\partial \theta}{\partial \zeta} = \frac{\theta_{m+1,n} - \theta_{m-1,n}}{2\Delta\zeta}.$$

The second derivatives in the boundary conditions for the vorticity were rewritten as

$$\frac{\partial^2 \Psi}{\partial \zeta^2} = 2\frac{\Psi_{2,n}}{(\Delta\zeta)^2} \quad \text{at} \quad \zeta = 0.$$

The adiabatic boundary conditions at $Y = 0$ and 1 were approximated by

$$\theta_{m,1} = \theta_{m,2} \quad \text{and} \quad \theta_{m,N+1} = \theta_{m,N}.$$

For the derivative of $\Omega$ with respect to time $Fo$ in equation (10), a pure implicit method was adopted. Equation (10) can be written by using a representation of differential operators

$$\mathrm{A}\Omega = \frac{\partial \Omega}{\partial Fo} + \mathrm{B}\theta + Pr\ \mathrm{C}\Omega. \tag{16}$$

When $\Delta Fo$ is used for the time interval and the time step is represented by a superscript $i$, an implicit type finite-difference equation for equation (16) can be written as

$$(\mathrm{A}^i - 1/\Delta Fo)\Omega^{i+1} = -\Omega^i/\Delta Fo + \mathrm{B}\theta^i + Pr\ \mathrm{C}\Omega^i. \tag{17}$$

Similarly equations (12), (13), and (11) can be written respectively as

$$\mathrm{D}^i\Psi^{i+1} = -\Omega^{i+1} + \mathrm{C}\Psi^i \tag{18}$$

$$U^{i+1} = \mathrm{E}\Psi^{i+1}, \quad V^{i+1} = \mathrm{F}\Psi^{i+1} \tag{19}$$

$$\mathrm{G}^{i+1}\theta^{i+1} = \mathrm{C}\theta^i. \tag{20}$$

Equations (17)–(20) are respectively changed to the set of finite-difference equations by using the above mentioned finite-difference formulae for the derivatives with respect to the space coordinates. Each set of simultaneous linear equations can be solved by the Gauss–Seidel iteration method. The criteria of convergence of the solution by the Gauss–Seidel iteration method are

$$\frac{\text{Max } |\Omega'_{m,n} - \Omega_{m,n}|}{\text{Max } |\Omega'_{m,n}|} < \varepsilon_\Omega$$

$$\frac{\text{Max } |\Psi'_{m,n} - \Psi_{m,n}|}{\text{Max } |\Psi'_{m,n}|} < \varepsilon_\Psi$$

$$\frac{\text{Max } |\theta'_{m,n} - \theta_{m,n}|}{\text{Max } |\theta'_{m,n}|} < \varepsilon_\theta$$

where primes denote the value at the next iteration step.

The steady-state solutions can be obtained by the following procedure. By using appropriate initial values of $\Omega^0$, $\theta^0$, $\Psi^0$, the values at the next time step are obtained by solving equations (17)–(20) in order. These calculations are iterated until the steady-state solutions are obtained. The criterion of the steady state is

$$\gamma = \frac{\text{Max } |\Omega^{i+1}_{m,n} - \Omega^{s,i+1}_{m,n}|}{\text{Max } |\Omega^{i+1}_{m,n}|} < 10^{-4}$$

where $\Omega^{s,i+1}$ is obtained by solving equation (17) from which two terms, $\Omega^{i+1}/\Delta Fo$ and $\Omega^i/\Delta Fo$, are removed. Therefore, $\Omega^{s,i+1}$ means the solution of the steady-state equation at the $(i+1)$th step. The time interval $\Delta Fo$ is determined according to the convergence criterion $\Delta Fo^*$ of the explicit finite-difference equation for equation (16)

$$\Delta Fo = \lambda \Delta Fo^* \quad (\lambda > 1).$$

The values of $\lambda$, $\varepsilon_\Omega$, $\varepsilon_\Psi$ and $\varepsilon_\theta$ were chosen appropriately depending on the value of $\gamma$ so that the computation time may be reduced. When $\gamma < 10^{-3}$, the following values were chosen: $\varepsilon_\Omega = \varepsilon_\Psi \leqslant 10^{-4}$ and $\varepsilon_\theta = \varepsilon_\Omega/10$. For a typical example, when $10^{-3} < \gamma < 10^{-2}$, $\varepsilon_\Omega = 10^{-3}$ and $\lambda = 20$.

2.3. *Procedure of analysis of the location of the melting front*

The location of the melting front at $\tau = \tau_j$ was approximated by the following polynomial function

$$F(Y,\tau_j) = \sum_{k=1}^{K-1} B_k(\tau_j)\left(Y^{k-1} - \frac{k-1}{K}Y^K\right). \quad (21)$$

Note that equation (21) satisfies $\partial F/\partial Y = 0$ at $Y = 1$. As the location of the melting front is known, the natural convection in the melt region can be analyzed. Therefore, the moving rate of the melting front at $\tau = \tau_j$ is determined by substituting the obtained temperature gradient at the melting front into the RHS of equation (14). By using an explicit representation, the location of the melting front at $Y = Y_n$ and $\tau = \tau_{j+1}$ is obtained by

$$F_n^{j+1} = F(Y_n,\tau_j) + \left[\frac{\partial F}{\partial \tau}\right](Y_n,\tau_j)\Delta\tau_j \quad (22)$$

where $\Delta\tau_j = \tau_{j+1} - \tau_j$.

The new location of the melting front at $\tau_{j+1}$ was determined by the least squares method. Namely the coefficients $B_k(\tau_{j+1})$ were determined so as to minimize

$$\sum_{n=1}^{N+1} \{F(Y_n,\tau_{j+1}) - F_n^{j+1}\}^2.$$

The initial location of melting front was determined from the exact solution for the Stefan problem [14]. Then $B_1(\tau_0) = 2\sigma\sqrt{(\tau_0/Ste)}$, $B_k(\tau_0) = 0$ $(k = 2, \ldots, K-1)$, where $\sigma$ is a root of the following equation

$$\sigma \exp(\sigma^2)\,\mathrm{erf}\,\sigma = Ste/\sqrt{\pi}. \quad (23)$$

## 3. RESULTS AND DISCUSSION

In order to confirm the validity of the present analysis, some calculations corresponding to the experimental conditions [7] were carried out. In the experiments [7] n-octadecane was used as a PCM. The heights of the PCM were $H = 15$ and 30 mm. The melting fronts were photographed at predetermined time intervals and the temperatures along the centerline of the enclosure were measured. The shapes of the melting front obtained both analytically and experimentally are plotted for the cases of $H = 15$ and 30 mm for different $Ra$ and $\tau$ in Figs. 2 and 3, respectively. In these calculations, the following values were chosen

$\tau_0 = 0.0005$, $K = 5$, $N = 30$

(for $H = 15$ mm), 50 (for $H = 30$ mm).

$M$ was changed depending on the location of the melting front and the Rayleigh number. For the case of Fig. 2(b), when $\tau \leqslant 0.015$, $M = 20$ and equation (7) were used; when $0.015 \leqslant \tau < 0.12$, $M = 20$ and equation (8); when $0.12 \leqslant \tau < 0.2$, $M = 30$ and equation (9); when $0.2 \leqslant \tau < 0.34$, $M = 40$ and equation (9). The time interval $\Delta\tau_j$ was chosen so that the rate of growth of the melting front to the width of the melt region might be less than 5%. As shown in Figs. 2 and 3, the analytical results agree well with the experimental ones. When the

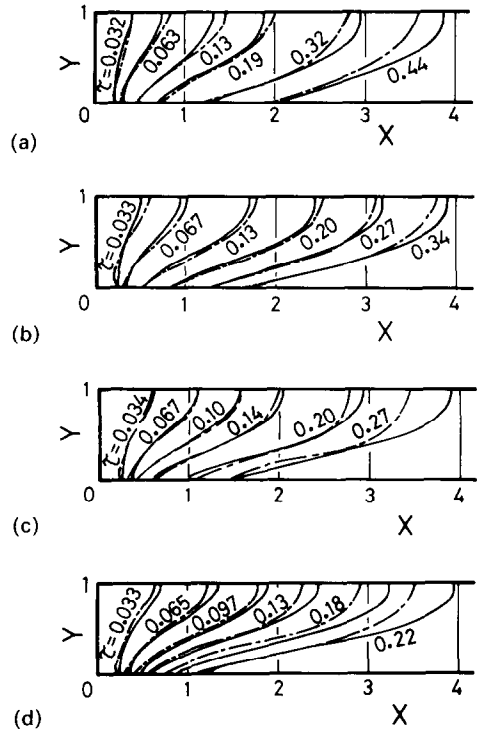


FIG. 2. Melting fronts as determined from the present analysis and photographs, $H = 15$ mm, $Pr = 56.2$: ——, analytical results; – – –, experimental results. (a) $Ra = 3.27 \times 10^5$, $Ste = 0.0451$; (b) $Ra = 6.95 \times 10^5$, $Ste = 0.0959$; (c) $Ra = 1.39 \times 10^6$, $Ste = 0.192$; (d) $Ra = 2.70 \times 10^6$, $Ste = 0.372$.

width to height ratio of the melt region in the case of $H = 15$ mm is large, the $X$ coordinates of the upper melting fronts determined from the analysis are greater than the experimental results. It is considered as a reason that in the experiments the heat loss from the top wall which

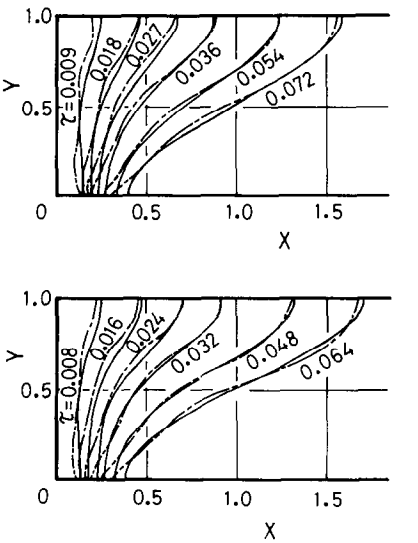


FIG. 3. Melting fronts as determined from the present analysis and photographs, $H = 30$ mm, $Pr = 56.2$: ——, analytical results; – – –, experimental results. (a) $Ra = 3.00 \times 10^6$, $Ste = 0.0517$; (b) $Ra = 5.34 \times 10^6$, $Ste = 0.0921$.

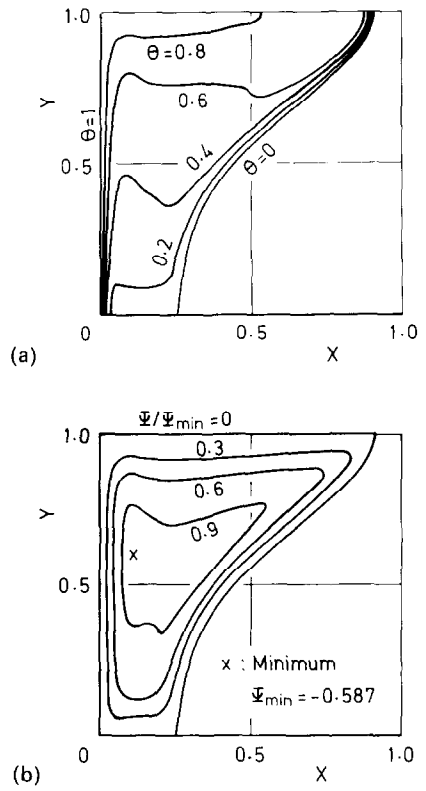


FIG. 4. Calculated temperature and stream function contours corresponding to Fig. 3(b), $Ra = 5.34 \times 10^6$, $\tau = 0.032$. (a) Temperature; (b) stream function.

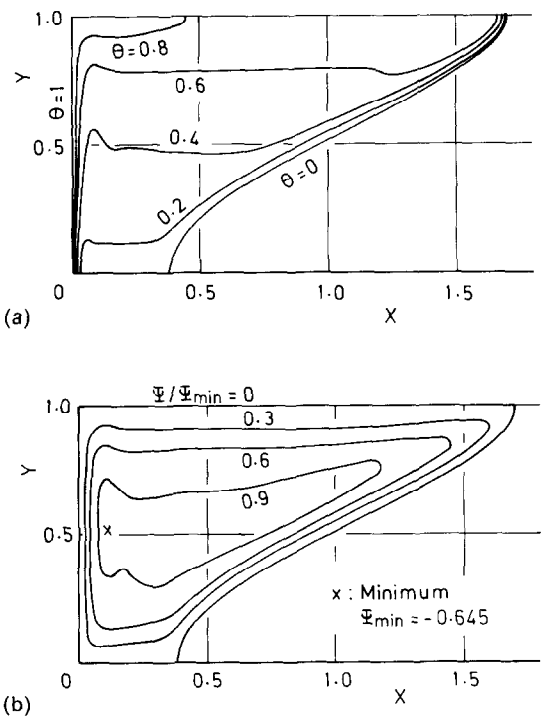


FIG. 5. Calculated temperature and stream function contours corresponding to Fig. 3(b), $Ra = 5.34 \times 10^6$, $\tau = 0.064$. (a) Temperature; (b) stream function.

was not perfectly insulated depressed the growth of the upper melting front.

The analytical results of the stream function and the temperature contour maps at $\tau = 0.032$ and 0.064 in Fig. 3(b) are shown in Figs. 4 and 5, respectively, as an example for high Rayleigh number. As an example for a large width to height ratio of the melt region, the calculated isotherms corresponding to Fig. 2(b) are shown in Fig. 6. The stream functions in Figs. 4(b) and 5(b) show that the flow in the melt region has a single recirculation zone. The flat distributions of the stream function around the central cores mean that the flow in the central region is stagnate. It is found from the concentration of the stream lines that the velocities along the vertical wall and the solid–liquid interface are higher than the velocities along both the horizontal walls. The stream lines near the vertical wall and the solid–liquid interface in Fig. 4(b) are similar to those in Fig. 5(b). In Figs. 4(a), 5(a) and 6, the spacing of the isotherms is close near the vertical wall and the solid–liquid interface but wide in the central core. The isotherms near the vertical wall are essentially the same at different times. This means that the heat transfer coefficient on the vertical wall is almost constant with time. Some isotherms, when they are considered as functions of $X$, have maximums near the heated vertical wall and/or minimums near the solid–liquid interfaces. This characteristic of isotherms is explained by the flow pattern as shown in Figs. 4(b) and 5(b). The maximum of the isotherms is caused by the upward flow of lower temperature liquid which has been cooled by the solid liquid interface.

The $Y$ component of velocity and temperature distributions along the centerline of the enclosure at various times for the case of Fig. 3(b) are shown in Fig. 7. In Fig. 7(b) the measured temperatures are also plotted. They agree well with the calculated temperature distributions. The gradients of both the velocity and temperature distributions near the vertical wall increase slightly with time. The central region in which both the distributions are flat expands with time, as it was found in the contour maps of Figs. 4–6.

The local Nusselt numbers on the vertical wall and the solid–liquid interface at substantially different times for the cases of Figs. 2(b) and 3(b) are shown in Fig. 8, where the heat transfer coefficient was defined based on the temperature difference ($T_W - T_F$). It is found from Fig. 8 that the local Nusselt number on the vertical wall increases slightly with time. On the other hand the local Nusselt number on the solid–liquid interface decreases considerably with time as the surface area of the solid–liquid interface increases.

The thermal energy stored as latent heat per unit depth of enclosure is determined from the area of the melt region as

$$Q_1 = \Delta h \rho \int_0^H f(y,t)\,\mathrm{d}y = \Delta h \rho H^2 \int_0^1 F(Y,\tau)\,\mathrm{d}Y.$$

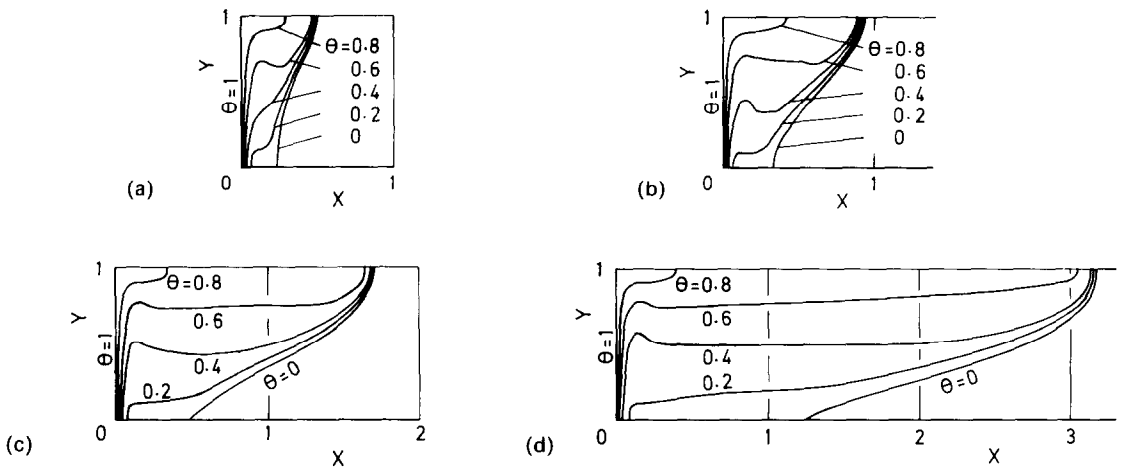


FIG. 6. Calculated isotherms corresponding to Fig. 2(b), $Ra = 6.95 \times 10^5$. (a) $\tau = 0.033$; (b) $\tau = 0.067$; (c) $\tau = 0.134$; (d) $\tau = 0.27$.

If a dimensionless thermal energy storage $Q_1^*$ is defined as

$$Q_1^* = Q_1/(\Delta h \rho H^2)$$

the $Q_1^*$ is equivalent to the dimensionless average width of the melt region defined by

$$\bar{F}(\tau) = \int_0^1 F(Y, \tau)\, dY. \tag{24}$$

If the steady-state temperature distribution of pure heat conduction is valid in the melt region, the following equations are obtained [14]

$$\Delta h \rho\, d\bar{f}/dt = k(T_W - T_F)/\bar{f} = \bar{h}(T_W - T_F).$$

Therefore, when $Ra = 0$

$$\bar{F} = \sqrt{(2\tau)}, \quad \overline{Nu} = \bar{h}H/k = 1/\bar{F} = 1/\sqrt{(2\tau)}. \tag{25}$$

The calculated results of equation (24) are shown in Fig. 9. In Fig. 9 the experimental results of $\bar{F}$ obtained by photographs are also shown. As can be noted, the analytical results of $\bar{F}$ agree well with the experimental results. As shown in Fig. 9, the dimensionless average

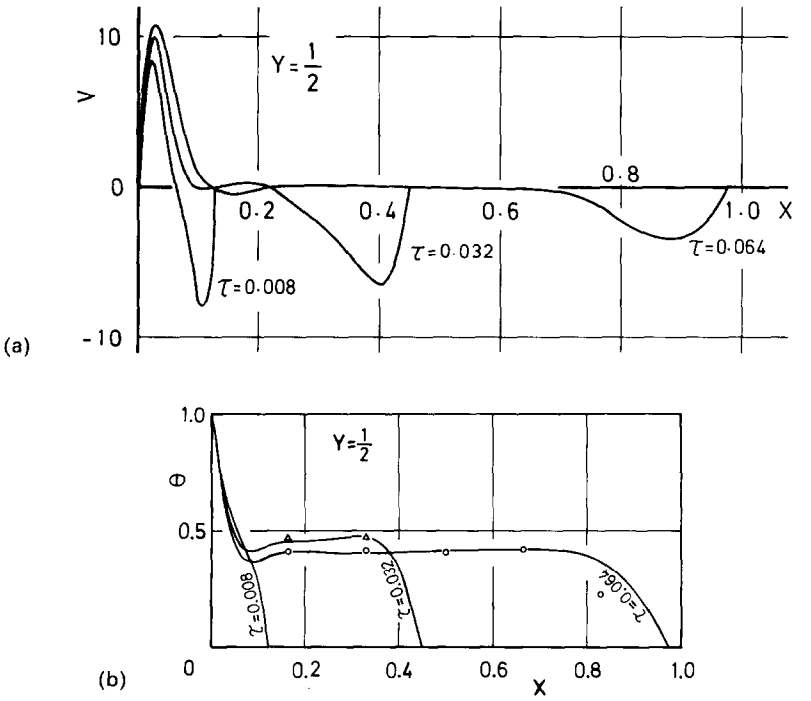


FIG. 7. Distributions of the $Y$ component of velocity and the temperature along centerline of the enclosure for the case of Fig. 3(b), $Ra = 5.34 \times 10^6$. (a) $Y$ component of velocity (analytical results); (b) temperature (——, analytical results; Δ, measured temperatures at $\tau = 0.032$; ○, measured temperatures at $\tau = 0.064$).

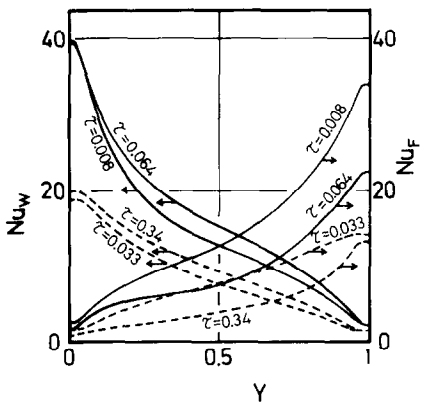


FIG. 8. Calculated local Nusselt numbers along the vertical wall and the solid–liquid interface for the cases of Fig. 2(b) ($Ra = 6.95 \times 10^5$) and Fig. 3(b) ($Ra = 5.34 \times 10^6$) (——, $Ra = 5.34 \times 10^6$; – – –, $Ra = 6.95 \times 10^5$).

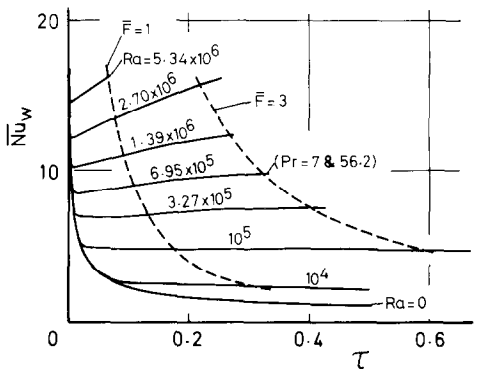


FIG. 10. Analytical results of the variation of the average Nusselt number on the vertical wall with dimensionless time τ, $Pr = 56.2$ (——, $\overline{Nu}_W - \tau$; – – –, lines of $\bar{F}$ = const.).

widths of the melt region increase almost linearly with dimensionless time τ after the quite early stages in which they coincide with the pure heat conduction solution, equation (25).

The variations of the average Nusselt numbers on the vertical wall with dimensionless time τ are shown by solid lines in Fig. 10. The broken lines in Fig. 10 show the lines on which the widths of the melt region have constant values. The calculations for the case of $Ra = 6.95 \times 10^5$ in Figs. 9 and 10 were carried out not only for $Pr = 56.2$ but also for $Pr = 7$. The results for both Prandtl numbers coincide extremely well with each other. As shown in ref. [8], the Prandtl number does not affect the melting rate for $Pr > 7$ when Rayleigh number is used. The average Nusselt numbers $\overline{Nu}_W$ coincide with the heat conduction solution, equation (25), in the early stage of melting. After the early stage, natural convection in the melt region dominates the melting process and the average Nusselt numbers vary linearly with dimensionless time. As the transition period from the conduction domain to the natural convection domain is very short, putting the transition time to $\tau_t$, the average Nusselt number on the vertical wall can be represented by

$$\begin{cases} \overline{Nu}_W = 1/\sqrt{(2\tau)} & \text{when} \quad \tau \leqslant \tau_t \\ \overline{Nu}_W = \overline{Nu}_{Wt}\{1 + C(\tau - \tau_t)\} & \text{when} \quad \tau > \tau_t \end{cases} \tag{26}$$

where

$$\overline{Nu}_{Wt} = 1/\sqrt{(2\tau_t)}. \tag{27}$$

The variations of the average Nusselt number $\overline{Nu}_W$ from $\tau_t$ to the time when $\bar{F} = 1$ are small and are within $\pm 12\%$ for $10^4 \leqslant Ra \leqslant 5 \times 10^6$. The analytical results of the average Nusselt numbers on the vertical wall are plotted in Fig. 11. The values at the transition time, $\overline{Nu}_{Wt}$, are shown by circles. The values at $\bar{F} = 1$ or 3 are also plotted in Fig. 11 using + and ×, respectively. The relationship correlating the experimental data for $3 \times 10^5 \leqslant Ra \leqslant 2 \times 10^7$ [7] is also shown by a broken line. This relationship based on the experiments has a good agreement with the analytical results. A straight line which represents well the average Nusselt numbers $\overline{Nu}_{Wt}$ was obtained as

$$\overline{Nu}_{Wt} = 0.234 Ra^{0.266} \quad (10^4 \leqslant Ra \leqslant 5 \times 10^6). \tag{28}$$

This is shown by a solid line in Fig. 11. Under the quasi-steady state assumption, the heat transferred from the vertical wall to the PCM is equal to the thermal energy stored as latent heat. Therefore, using the dimensionless parameters

$$\frac{d\bar{F}}{d\tau} = \overline{Nu}_W. \tag{29}$$

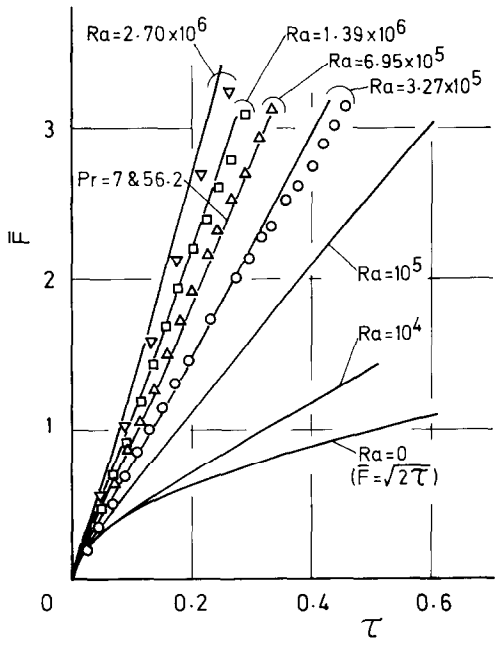


FIG. 9. Variation of the dimensionless average width of the melt region with dimensionless time (——, analytical results; ○, experimental results corresponding to Fig. 2(a); △, to Fig. 2(b); □, to Fig. 2(c); ▽, to Fig. 2(d)), $Pr = 56.2$.

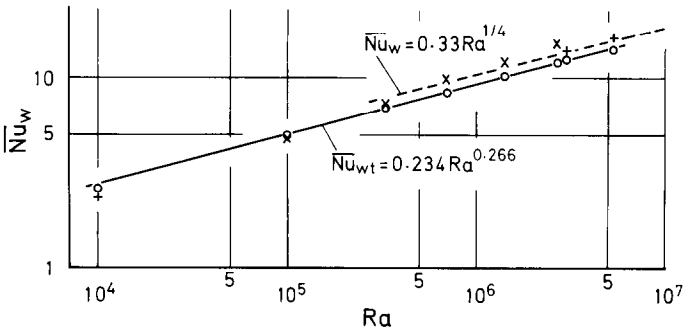


FIG. 11. Average Nusselt number on the vertical wall (analytical results: ○, at the transition time; +, when $\bar{F} = 1$; ×, when $\bar{F} = 3$; ——, equation (28); – – –, relationship determined from experiments [7]).

Substituting equation (26) into equation (29) and solving equation (29) yields

$$\begin{cases} \bar{F} = \sqrt{(2\tau)} & (\tau \leqslant \tau_t) \\ \bar{F} = \sqrt{(2\tau_t) + \overline{Nu}_{wt}(\tau - \tau_t)\{1 + C(\tau - \tau_t)/2\}} & (\tau > \tau_t) \end{cases} \tag{30}$$

where $\tau_t$ is obtained from equations (27) and (28). The coefficient $C$ obtained from Fig. 11 is shown in Fig. 12. Neglecting $C$ in equation (30) for the case of $Ra = 2.7 \times 10^6$ in Fig. 9 yields only a 14% lower value of $\bar{F}$ than the value in Fig. 9 at $\tau = 0.25$.

## 4. CONCLUDING REMARKS

The melting process of a horizontal plate-like solid heated from a vertical wall was analyzed by means of a finite-difference method. The analytical results were compared with the experimental results using n-octadecane as a phase change material. The results of this study lead to the following conclusions.

(1) The good agreement between the analytical and experimental results indicates that the present analytical method which uses the quasi-steady state assumption and the two-step variable transformation technique is available.

(2) In the quite early stage of melting, pure heat conduction dominates the melting process. After this early stage, natural convection in the melt region dominates it.

(3) In the period of the natural convection domain, the average Nusselt number on the vertical wall varies linearly with the dimensionless time but its variation is small. Therefore, the dimensionless thermal energy stored as latent heat varies almost linearly with the dimensionless time.

(4) The average Nusselt number on the solid–liquid interface decreases with the dimensionless time as the surface area of the solid–liquid interface increases.

(5) Both the average Nusselt number on the vertical wall and the dimensionless thermal energy stored as latent heat were expressed by simple relationships with Rayleigh number and the dimensionless time.

(6) As shown in ref. [8] concerning the melting around a vertical cylinder, the Prandtl number does not affect the melting rate for $Pr \geqslant 7$ when the Rayleigh number is used.

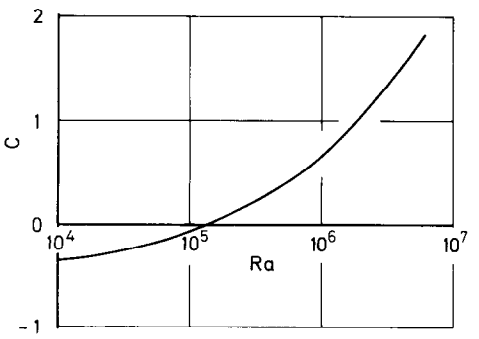


FIG. 12. Coefficient $C$ in equations (26) and (30).

## REFERENCES

1. A. G. Bathelt, R. Viskanta and W. Leidenfrost, An experimental investigation of natural convection in the melted region around a heated horizontal cylinder, *J. Fluid Mech.* **90**(2), 227–239 (1979).
2. E. M. Sparrow, R. R. Schmidt and J. W. Ramsey, Experiments on the role of natural convection in the melting of solids, *Trans. Am. Soc. Mech. Engrs*, Series C, *J. Heat Transfer* **100**, 11–16 (1978).
3. A. G. Bathelt and R. Viskanta, Heat transfer at the solid–liquid interface during melting from a horizontal cylinder, *Int. J. Heat Mass Transfer* **23**, 1493–1503 (1980).
4. E. M. Sparrow and J. A. Broadbent, Inward melting in a vertical tube which allows free expansion of the phase-change medium, *Trans. Am. Soc. Mech. Engrs*, Series C, *J. Heat Transfer* **104**, 309–315 (1982).
5. N. W. Hale, Jr. and R. Viskanta, Photographic observation of the solid–liquid interface motion during melting of a solid heated from an isothermal vertical wall, *Lett. Heat Mass Transfer* **5**, 329–337 (1978).
6. P. D. Van Buren and R. Viskanta, Interferometric measurement of heat transfer during melting from a vertical surface, *Int. J. Heat Mass Transfer* **23**, 568–571 (1980).
7. M. Okada, Melting from a vertical plate between insulated top and bottom surfaces, *Proc. ASME/JSME Thermal Engng Joint Conf.*, Vol. 1, pp. 281–288. American Society of Mechanical Engineers (1983).

8. E. M. Sparrow, S. V. Patankar and S. Ramadhyani, Analysis of melting in the presence of natural convection in the melt region, *Trans. Am. Soc. Mech. Engrs*, Series C, *J. Heat Transfer* **99,** 520–526 (1977).
9. H. Rieger, U. Projahn and H. Beer, Analysis of the heat transport mechanisms during melting around a horizontal circular cylinder, *Int. J. Heat Mass Transfer* **25,** 137–147 (1982).
10. T. Saito and K. Hirose, High Rayleigh number solutions to problems of latent heat thermal energy storage in a horizontal cylinder capsule, *Trans. Am. Soc. Mech. Engrs*, Series C, *J. Heat Transfer* **104,** 545–553 (1982).
11. A. Saito, Y. Utaka, K. Katayama and H. Matsui, A study on the heat transfer of latent heat thermal energy storage (1st report, Removal and storage characteristics of the latent heat TES capsule), *Trans. Japan Soc. Mech. Engrs* **B49,** 843–851 (1983).
12. L. S. Yao and F. F. Chen, Effects of natural convection in the melted region around a heated horizontal cylinder, *Trans. Am. Soc. Mech. Engrs*, Series C, *J. Heat Transfer* **102,** 667–672 (1980).
13. P. J. Roache, *Computational Fluid Dynamics* (Revised edn.), p. 73. Hermosa, Albuquerque, New Mexico (1976).
14. H. S. Carslaw and J. C. Jaeger, *Conduction of Heat in Solids* (2nd edn.), p. 286. Oxford University Press, London (1959).

## ANALYSE DU TRANSFERT THERMIQUE PENDANT LA FUSION D'UNE PAROI VERTICALE

**Résumé**—Une frontière verticale d'un solide en forme de plaque horizontale, initialement à la température de fusion (avec des surfaces supérieure et inférieure adiabatiques) est soumise à un échelon accroissement de température. Le mécanisme de fusion avec convection naturelle et la région de fusion variable dans le temps sont analysés au moyen d'une méthode aux différences finies. Les résultats analytiques sur la forme du front du fusion et sur la distribution de température dans la région de fusion s'accordent bien avec les résultats expérimentaux, en utilisant du x-octadécane comme matériau à changement de phase, présentés par l'auteur. Une formule simple entre le nombre de Nusselt moyen le long de la paroi verticale et un temps adimensionnel est obtenue.

## ANALYSE DER WÄRMEÜBERTRAGUNG WÄHREND DES SCHMELZENS EINER VERTIKALEN WAND

**Zusammenfassung**—Eine vertikale Begrenzungsfläche eines horizontalen plattenartigen Festkörpers, dessen Ober- und Unterseite adiabat sind und der sich zu Beginn auf Schmelztemperatur befindet, wird einer schrittweisen Temperaturerhöhung unterworfen. Der resultierende Schmelzprozeß mit natürlicher Konvektion in der zeitlich veränderlichen Schmelzzone wird mit der Methode der finiten Differenzen analysiert. Die berechnete Form der Schmelzfront und die Temperaturverteilung in der Schmelzzone stimmen gut mit den experimentellen Ergebnissen überein, die mit n-Oktadecan ermittelt wurden. Der Autor berichtete darüber. Eine einfache Beziehung zwischen der mittleren Nusselt-Zahl entlang der vertikalen Wand und der dimensionslosen Zeit wurde aufgestellt.

## АНАЛИЗ ТЕПЛОПЕРЕНОСА ОТ ВЕРТИКАЛЬНОЙ СТЕНКИ ПРИ ПЛАВЛЕНИИ

**Аннотация**—Боковая грань твердого тела, имеющего форму горизонтальной пластины, с адиабатическими верхней и нижней поверхностями, находящаяся первоначально при температуре плавления, подвергалась ступенчатому нагреву. Возникающий в результате процесс плавления с естественной конвекцией в зоне расплава исследовался конечно-разностным методом. Результаты аналитического определения формы фронта плавления и распределения температуры в зоне расплава хорошо согласуются с экспериментальными данными, полученными при использовании n-октадекана в качестве материала, претерпевающего фазовое превращение. Получена простая зависимость между средним значением числа Нуссельта вдоль вертикальной стенки и безразмерным временем.